High-Water Alerts from Coinciding High Astronomical Tide and High Mean Sea Level Anomaly in the Pacific Islands Region

SCOTT A. STEPHENS, ROBERT G. BELL, DOUGLAS RAMSAY, AND NIGEL GOODHUE

National Institute of Water and Atmospheric Research, Hillcrest, Hamilton, New Zealand

(Manuscript received 3 February 2014, in final form 27 August 2014)

ABSTRACT

A technique to produce high-water alerts from coinciding high astronomical tide and high mean sea level anomaly is demonstrated for the Pacific Islands region. Low-lying coastal margins are vulnerable to episodic inundation that often coincides with times of higher-than-normal high tides. Prior knowledge of the dates of the highest tides can assist with efforts to minimize the impacts of increased exposure to inundation. It is shown that the climate-driven mean sea level anomaly is an important component of total sea level elevation in the Pacific Islands region, which should be accounted for in medium-term (1–7 months) sea level forecasts. An empirical technique is applied to develop a mean sea level–adjusted high-water alert calendar that accounts for both sea level components and provides a practical tool to assist with coastal inundation hazard planning and management.

1. Introduction

Coastal inundation events damage infrastructure and property, cause economic loss and disruption, and put lives at risk. Forecasts of the timing and magnitude of coastal hazards allow coastal or emergency managers to design appropriate responses in advance that can significantly reduce risk. Here we discuss a method for the development of high-water calendars to provide alerts for dates of very high tides compounded by high background mean sea level anomaly (MSLA), as a practical prewarning tool to assist with management of potential coastal inundation events. While a high-tide alert calendar can be derived from knowledge of tides alone, the inclusion of MSLA enhances the prediction of high-water alert levels, with a more realistic connection to what actually may occur. The high-water peak elevation modulates the potential impact of other compounding processes such as swell waves and/or storm surge.

The focus of the study is on the Pacific Island region (PIR), which has a high exposure to sea level rise due to coastal zones with dense populations, low land elevations, and in some cases subsidence, and/or inadequate adaptive capacity (Nicholls and Cazenave 2010; Nurse et al. 2014). These same factors also make the Pacific Island region vulnerable to abnormally high sea levels. Although some Pacific Islands away from the equator are exposed to tropical cyclones with potentially devastating consequences (e.g., Chu and Wang 1998; Diamond et al. 2012; Sinclair 2002; Terry and Gienko 2010), many locations suffer regular exposure to high sea level and inundation during the dates of the highest high tides, as the high tides increase exposure to the impact of other compounding processes such as swell waves (Hoeke et al. 2013). Furthermore, locations within the PIR have substantial fluctuations in MSLA due to the El Niño–Southern Oscillation (ENSO) phenomenon; El Niño/La Niña events correspond to sea level lows/highs of ±0.2–0.3 m compared to neutral conditions (Becker et al. 2012). Along with the tide, these positive MSLA fluctuations further precondition the exposure to coastal inundation.

Tsunami and land subsidence aside, there are several meteorological and astronomical influences on sea level that can combine in a number of ways to inundate low-lying coastal margins: the height of mean sea level (MSL) relative to a local datum or landmark, astronomical tides (hereinafter called tide), synoptic weather-induced storm-surge, wave setup and run-up, MSLA (caused by seasonal, interannual, and interdecadal climate variability), and long-term change in MSL through sea level rise. It is common to treat the wave-induced setup and run-up separately from

Corresponding author address: Scott A. Stephens, National Institute of Water and Atmospheric Research, P.O. Box 11-115, Hillcrest, Hamilton 3251, New Zealand.
E-mail: scott.stephens@niwa.co.nz

DOI: 10.1175/JTECH-D-14-00027.1

the still (nonwave)-water level because sea level gauges are usually placed inside harbors to minimize the effects of wave setup and run-up. Nevertheless, at most gauge locations there will still be a wave setup component in the measured storm surge that cannot be separated analytically because wave setup is aliased with storm surge (where storm surge is a weather-induced component of the still-water level due to inverse-barometer and wind setup, but not wave breaking). We use the term MSLA in recognition that the anomaly is calculated relative to MSL, after MSL and any long-term sea level trend has been removed (described later).

The tide is the largest contributor to sea level variability and to annual maximum sea level elevation (relative to MSL), in both New Zealand (Bell 2010) and the PIR (Merrifield et al. 2013; Timmermann et al. 2010), notwithstanding the effects of episodic extreme storms that occur less than once per year on average. The high-water alert calendar builds on the concept of alerting coastal managers to precalculated ''red alert'' days when high-tide peaks are predicted to be unusually high (Bell 2010). An analysis of historical storm-tide events in New Zealand showed that extreme storm-tide levels around the open coast of New Zealand are dominated by very high tides coinciding with small-to-moderate storm surges, compounded often by high background MSLA. This led to the development of a simple storm-tide ''forecasting'' approach, which is a prepublished list each year of red-alert days when high perigean spring tides are predicted (see http://www.niwa.co.nz/natural-hazards/physical-hazards-affecting-coastal-margins-and-the-continental-shelf/storm-tide-red-alert-days-2014). The red-alert concept works in New Zealand because the semidiurnal tides dominate sea level variability and storm surges are limited to ≤ 1 and mostly <0.6 m, which is approximately 25% of the average tidal range. Coastal or hazard managers are advised to keep a close watch on the weather for lower barometric pressure and adverse winds during the red-alert tide days, as even a minor storm could lead to the inundation of low-lying areas, especially if accompanied by swell (Bell 2010). For example, the highest storm tide in Auckland, New Zealand, on record since 1903 occurred on 23 January 2011, closing major city highways and causing millions of dollars of flood-related damage. At 0.4 m the surge was only moderate, but it coincided with a predicted red-alert tide and a background MSLA of nearly 0.1 m (25% of the storm surge).

Tides result from the gravitational attraction of the moon and sun; they are deterministic and can be predicted using analytical methods such as tidal harmonic analysis (Foreman et al. 2009) based on well-established tidal theory (e.g., Pugh 2004). With the exception of the solstice tides that are aliased with atmospheric and steric effects on sea level, tidal harmonic constituents remain relatively stationary from year to year, with amplitude variability ≤ 0.02 m at the locations analyzed. Although there is evidence for long-term change in ocean tide amplitudes in some regions, the changes of only a few percent per century (Jay 2009; Müller 2011; Rasheed and Chua 2014; Woodworth 2010) do not affect the tidal predictions of a few months to a year required to construct a high-water alert calendar.

Changes in MSLA are related to regional wind and steric changes. Changes in ocean temperature and salinity affect sea level through the associated changes in density and volume, and wind stress is a main driver of changes in mass and steric height through dynamic processes. These changes are directly related to coupled climate modes of variability, such as ENSO (Stammer et al. 2013). Several studies have shown that low-frequency (ENSO scale and multidecadal) MSLA can be correlated to various climate indices (Becker et al. 2012; Chowdhury et al. 2007; Merrifield et al. 2012; Miles et al. 2014; Sasaki et al. 2008). The ENSO phenomenon has a strong impact on MSLA in the western Pacific Islands region with a tendency for lower mean sea levels during El Niño events and higher mean sea levels during La Niña events. Pacific Islands west of the date line show particularly high mean sea levels during La Niña periods (Becker et al. 2012; Miles et al. 2014), and during such periods the frequency and magnitude of high-tide-modulated flooding is much greater. MSLA forecasts from 0 to 7 months in advance are available within the PIR. Present examples in the Pacific Islands region are MSLA forecasts between 40°S and 40°N (Miles et al. 2014) and 3-month seasonal outlooks at U.S.-affiliated Pacific Islands (Chowdhury et al. 2007). Miles et al. (2014) obtained statistically significant correlations at lead times of up to 7 months for both winter and summer seasons in the Pacific basin, observing relatively high predictive skill in this region due to the strength and predictability of ENSO, which delivers the dominant MSLA seasonal signal at both the global mean and regional scale. The predictive skill increases with reducing lead time.

This paper shows how high-water alert thresholds can be built into a high-water calendar that includes both tide and MSLA predictions, as a practical tool to predict dates of abnormally high tides. The method section introduces the concept of high-water exceedance curves and their use to define alert thresholds for high-water elevations, relative to a local vertical datum. The sea level records and their decomposition into tide and MSLA are described, along with the treatment of the mean seasonal sea level cycle that has both tidal and nontidal components. The results section examines the interaction of tide and MSLA to establish a statistical basis for the calculation of high-water exceedance

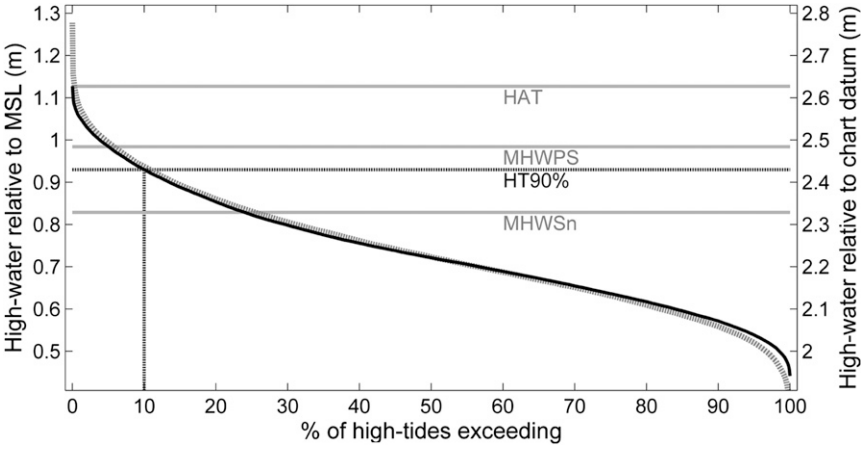

FIG. 1. High-tide exceedance curve for Moturiki based on 1974–2012 predicted high tides. The bold curve indicates high tide alone and the light curve indicates high tide plus MSLA (high water). Refer to text for definition of the various tide levels and MSL.

thresholds. The relative influence of tide and MSLA is demonstrated for various MSLA and tide regimes. Finally, the high-water alert calendar is demonstrated for two locations contrasting a relatively large tidal influence with a relatively large MSLA influence. Results are then discussed and conclusions drawn.

2. Method

a. High-water exceedance curves

The New Zealand red-alert tide calendar alerts a user to times when high-tide peaks equal or exceed the sum of the amplitudes of the three largest tidal harmonics, otherwise known as mean high-water perigean springs (MHWPS), M_2 (principal lunar semidiurnal) + S_2 (principal solar semidiurnal) + N_2 (larger lunar elliptic semidiurnal). In New Zealand, the intersection of the mean high-water springs (MHWS) elevation with the land defines the landward jurisdictional boundary of the coastal marine area, yet MHWS can be defined in different ways such as the prior MHWPS definition, or the nautical definition of MHWSn = M_2 + S_2, for example (Pugh 1987). Despite New Zealand's tidal regime being semidiurnal (with small diurnal constituents), there is a contrast between the west and east coasts. The west coast tides are dominated by M_2 + S_2, leading to fortnightly spring and neap tides of approximately equal amplitude, whereas on the east coast the tidal regime is dominated by the 27.5-day cycle of perigean and apogean tides and a single dominant spring tide per month, because the S_2 solar tide degenerates to low amplitudes (Walters et al. 2001). Because of the variability in tide regimes, definitions of MHWS (or red-alert elevations) can be inconsistent when tide characteristics vary substantially around the New Zealand coast. Bell (2010) showed that high-tide exceedance curves, based on the cumulative distribution function (CDF) of long-term tide predictions, allow MHWS to be consistently defined based on a common exceedance threshold that is independent of tide regime. Here, we apply the tide exceedance method to determine alert thresholds for high tides and high tide plus MSLA (high water), which, while demonstrated for a New Zealand site, can apply to any other country.

Figure 1 shows a high-tide exceedance curve for Moturiki Island (New Zealand), based on tidal harmonic predictions from 1974 to 2012. The tide exceedance curve changes little for tide predictions longer than a nodal cycle (18.6 years). MHWSn, MWHPS, and the highest astronomical tide (HAT) elevations are marked, along with the 90% cumulative exceedance threshold (HT90%), which is equaled or exceeded only by the largest 10% of all high tides [defined by Bell (2010) as MHWS-10]. The high-tide exceedance curve can be used to determine the high-tide height associated with any exceedance probability—for example, the 95th and 99th percentiles (HT95% and HT99%, respectively; not marked)—independently of tidal regime and associated MHWS definitions. The tide exceedance curve is shown here relative to MSL = 0 (excluding all other sea level components and sea level rise) on the left-hand axis, and relative to chart datum including 1993–2012 MSL on the right-hand axis; the conversion is explained later.

Exceedance curves can be defined for any sea level component individually or for the sum of more than one sea level component. They provide a framework for combining high tide and MSLA to identify the joint probability of exceedance of combined high-water elevations. The exceedance curve for the empirical distribution of combined high water with MSLA is also marked in Fig. 1. The

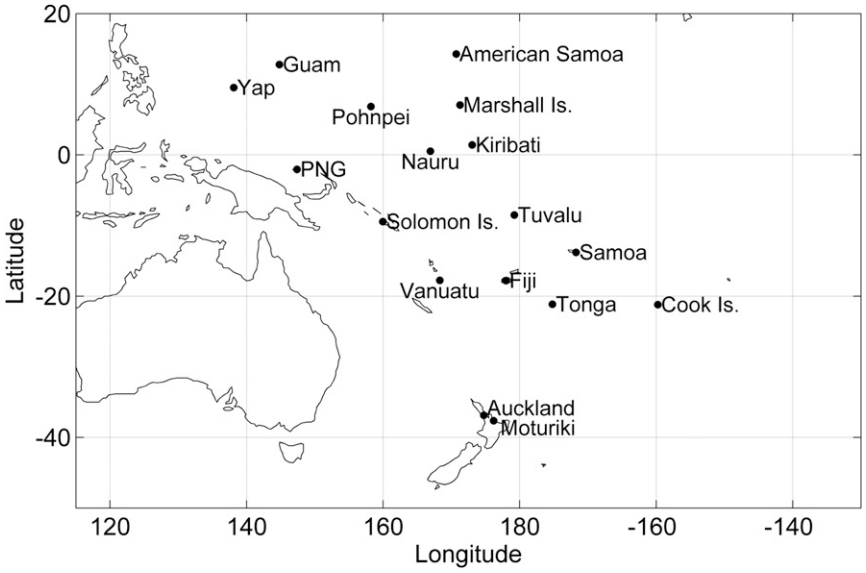

FIG. 2. Map of the Pacific Ocean showing locations of sea level gauges used for this study, within the PIR and New Zealand.

high-water exceedance distribution includes higher combined sea level elevations than the high-tide distribution alone. However, the position of the high-water exceedance curve is based around the high-tide curve that is offset positively from zero. Thus, the high-tide exceedance curve can be thought of as the "base" and the inclusion of MSLA as a "compounding effect." At low (and high) exceedance probabilities, the exceedance curves asymptote toward high (and low) "tails." The combination of the high tails leads to greater departures of the high-water curve from the high-tide curve at low exceedance probabilities. Thus, while the high-water curve mostly tracks the high-tide curve, it rises substantially higher at very low exceedance thresholds (e.g., red alert).

The high-water exceedance curve is simply the cumulative distribution function of the sum of the tide and MSLA time series; thus, it is empirically based. The joint probability of high tide and MSLA is not modeled here, nor do we assume that tide and MSLA are independent—as shown below the tide and MSLA covary. Nevertheless, as shown later, the assumption of independence is a reasonable approximation when calculating high-water alert thresholds.

b. *Definition of alert threshold*

The aim of the red-alert tide calendar is to alert end users to dates of unusually large high waters. In New Zealand this is based on the aforementioned MHWPS elevation, and dates of higher tides are colored red on the calendar. The approach is amenable to setting high-tide alert thresholds that preserve a specified percentage of high-tide exceedances between sites, but it requires a practical choice of threshold. An ideal alert threshold would represent an elevation that coincides with a substantial chance of consequential inundation when it is exceeded. It would also be low enough to provide a substantial number of alert dates, given that increased hazard exposure to inundation (due to high tide plus MSLA) will not always coincide with other coastal hazard drivers, such as swell waves for example.

Alert thresholds can be chosen relative to a local benchmark or a coastal feature such as a wharf or seawall, since the consequences of coastal inundation are location specific (e.g., low-relief topography behind a coastal barrier compared with steeply rising topography). In practice, coastal morphology, such as beaches, rock platforms, and coral reefs, tend to naturally adapt to prevailing sea conditions (in the absence of human infrastructure), with the MHWS elevation plus an allowance for wave setup and/or MSLA approximating the land–sea boundary (Boak and Turner 2005). Thus, sea level elevations above a pragmatic MHWS are beginning to encroach on "land" and any adjacent human infrastructure.

To relate the high-tide alert thresholds to local fixed survey data or landmarks, MSL must first be determined relative to local benchmarks or landmarks. This is achieved by averaging nontidal sea level elevation measurements relative to local benchmarks over a long time period, usually several years to average out seasonal influences. The known MSL data offset is then added to the high-tide alert thresholds that are determined relative to MSL = 0 (Fig. 1).

On New Zealand's northeastern coast (e.g., at Moturiki and Auckland; Fig. 2), approximately 36 out of 706 high

TABLE 1. Sea level records used in the study. Longitudes are given in °E, negative longitudes are equivalent to °W, and negative latitudes are equivalent to °S.

Site No.	Location	Lat (°N)	Lon (°E)	Start date	End date
1	Fiji (Viti Levu–Lautoka)	−17.80	178.00	24 Oct 1992	31 May 2014
2	Auckland (New Zealand)	−36.84	174.74	1 Jan 1970	31 May 2011
3	Marshall Islands (Majuro–Uliga)	7.07	171.26	14 May 1993	31 May 2014
4	Moturiki (New Zealand)	−37.63	176.19	1 Jun 1974	31 Dec 2012
5	Samoa (Upolu–Apia)	−13.80	−171.75	27 Feb 1993	31 May 2014
6	Kiribati (Tarawa–Betio)	1.42	173.03	3 May 1974	30 Jul 2012
7	Tonga (Tongatapu–Nuku'alofa)	−21.13	−175.20	21 Jan 1993	31 May 2014
8	American Samoa (Pago Pago)	14.28	170.70	31 Jul 1966	31 Dec 2012
9	Tuvalu (Funafuti–Fongafale)	−8.50	179.22	24 Mar 1993	30 Apr 2014
10	Nauru (Aiwo)	0.53	166.93	7 May 1974	31 Jul 2012
11	Vanuatu (Efate–Port Vila)	−17.75	168.30	15 Jan 1993	31 May 2014
12	Papua New Guinea (Manus–Lombrom)	−2.04	147.37	29 Sep 1994	31 May 2014
13	Pohnpei–Dekehtik (Federated States of Micronesia)	6.85	158.22	21 Apr 1974	31 Jul 2012
14	Yap (Federated States of Micronesia)	9.53	138.12	10 May 1969	30 Jun 2012
15	Solomon Islands (Guadalcanal–Honiara)	−9.44	159.95	28 Jul 1994	31 May 2014
16	Cook Islands (Rarotonga–Avarua)	−21.20	−159.77	24 Apr 1977	31 Aug 2011
17	Guam (Apra Harbor)	12.80	144.80	10 Mar 1948	31 Dec 2008

tides equal or exceed the MHWPS elevation per year, or about 5% of all high tides. Therefore, a 95th percentile elevation threshold would approximately equal the MHWPS-based red-alert calendar at Moturiki and Auckland—this alert threshold has proven to be pragmatic in New Zealand. These MHWPS high tides commonly occur in clusters over 2–4-day periods, with clusters occurring 8–9 times per year on average. The 95th percentile of the empirical distributions is used in examples below, but note that other similar high-percentile thresholds could be used. The high-tide alert calendar is also demonstrated using 90th, 95th, and 99th percentile elevation thresholds. The provision of several alert thresholds can allow end users in time to develop a sense of the consequence of exceedance of the various thresholds. The 90% exceedance yellow-alert level equates to exceedance by approximately three high-tide peaks on average per fortnight in a semidiurnal tidal regime, so it represents a higher sea level that is relatively regularly exceeded. The 90% exceedance rate is similar to the MHWS occurrence rate in a semidiurnal tidal regime (Bell 2010). The 99% exceedance red-alert level can be expected to be exceeded during approximately seven high-tide peaks per year on average, so it is an occasionally exceeded level. Figure 1 shows that sea levels that exceed the red-alert threshold are in the high tail of the joint probability CDF and usually involve simultaneous occurrences of both high tides and high MSLA.

c. *Sea level records*

Sea level gauge data were obtained from 15 locations within the Pacific Island region, plus two New Zealand sites (Fig. 2; Table 1). The analyzed gauges do not include all of the available sea level records in the PIR, but were chosen to represent locations throughout the region and to include a variety of tide regimes and relative MSLA variability; the 15 locations provide sufficient variability to demonstrate the MSLA-plus-high-tide alert calendar concept. The two New Zealand sites were included because of the relatively low MSLA variability relative to tide range and because the authors are familiar with the application of the red-alert tide calendar there. Moturiki has New Zealand's longest open-coast sea level gauge record (40 years), and nearby Auckland has one of New Zealand's longest and most complete sea level records, spanning back to 1900.

Hourly sea level data were downloaded from the University of Hawaii Sea Level Center's (UHSLC) website (http://uhslc.soest.hawaii.edu/data/download/rq) and the Australian Bureau of Meteorology's (BOM) South Pacific Sea Level and Climate Monitoring Project (SPSLCMP) website (http://www.bom.gov.au/oceanography/projects/spslcmp/data). Moturiki data were obtained from the National Institute of Water and Atmospheric Research (NIWA) and Auckland data from the Port of Auckland.

The analyzed sea level records covered different epochs. Using data from the same epoch is crucial for some quantitative intersite comparisons, such as determination and intercomparison of MSL between sites. However, for our purposes it is sufficient to make qualitative intersite comparisons between tide and the MSLA regime and high tide–MSLA interaction. The BOM gauge records begin in 1992 and 1993, whereas other records are longer and thus provide more data for comparing the site-specific tide-

TABLE 2. Statistics of tide and MSLA at 17 locations. The data are sorted according to the ascending ratio of the 95th percentile of MSLA/high tide. The tidal and MSLA range was defined in terms of the difference between the 0.5 and 99.5 percentiles of each record.

Location	Tide regime	Largest three tidal constituents (name amplitude)			Tide range (m)	HT95%	MSLA range (m)	MSLA95%	MSLA95%/HT95%
Fiji	Semidiurnal	M_2 0.63	S_2 0.15	N_2 0.15	1.95	0.96	0.18	0.06	6
Auckland	Semidiurnal	M_2 1.15	N_2 0.23	S_2 0.18	3.13	1.57	0.27	0.1	7
Marshall Islands	Semidiurnal	M_2 0.52	S_2 0.28	N_2 0.1	1.85	0.95	0.21	0.08	8
Moturiki	Semidiurnal	M_2 0.73	N_2 0.16	S_2 0.1	1.98	0.98	0.25	0.09	9
Samoa	Semidiurnal	M_2 0.39	N_2 0.11	S_2 0.09	1.22	0.62	0.25	0.06	10
Kiribati	Semidiurnal	M_2 0.58	S_2 0.3	N_2 0.12	2.07	1.06	0.39	0.12	11
Tonga	Semidiurnal	M_2 0.51	N_2 0.12	K_1 0.07	1.47	0.73	0.23	0.08	11
American Samoa	Semidiurnal	M_2 0.38	N_2 0.10	S_2 0.06	1.12	0.57	0.20	0.07	11
Tuvalu	Semidiurnal	M_2 0.58	S_2 0.25	N_2 0.14	1.99	1.00	0.48	0.13	13
Nauru	Semidiurnal	M_2 0.54	S_2 0.3	K_1 0.14	2.02	1.04	0.49	0.14	14
Vanuatu	Mixed	M_2 0.36	K_1 0.16	S_2 0.11	1.33	0.59	0.25	0.09	15
Papua New Guinea	Diurnal	K_1 0.23	O_1 0.15	M_2 0.1	0.96	0.39	0.19	0.06	16
Pohnpei	Semidiurnal	M_2 0.27	S_2 0.19	K_1 0.16	1.24	0.69	0.45	0.12	18
Yap	Mixed	M_2 0.4	K_1 0.19	S_2 0.14	1.51	0.64	0.49	0.17	27
Solomon Islands	Diurnal	K_1 0.22	O_1 0.11	S_2 0.07	0.85	0.39	0.30	0.11	29
Cook Islands	Semidiurnal	M_2 0.27	S_2 0.07	N_2 0.06	0.81	0.41	0.33	0.12	29
Guam	Mixed	M_2 0.22	K_1 0.16	O_1 0.12	0.95	0.35	0.47	0.14	41

plus-MSLA regimes. The use of available records is consistent with the concept of using the empirical record to define high-tide alert thresholds. An application of the method at Kosrae, in the Federated States of Micronesia, is discussed later to demonstrate this concept.

The raw sea level records were decomposed into tide and MSLA components as follows, and the method is consistent with Goring et al. (2011):

1) The Moturiki and Auckland raw sea level records were decimated to 1-h intervals to match the UHSLC and SPSLCMP records. This is not strictly necessary, but sea level data decimated to 1 h is sufficient to enable accurate tidal harmonic analysis and to determine MSLA. Decimation reduces the datasets, making processing more efficient. Hourly data does not resolve some high-frequency sea level motion, such as seiching or wave-induced fluctuation, which can have periods of motion of less than 1 h, but those processes are not considered in the high-water calendar.
2) The tidal motion was resolved using tidal harmonic analysis, following Foreman et al. (2009). Along with tidal harmonic analysis, this software also fits a mean and a linear trend through the raw data. The tide was predicted relative to a mean sea level of zero, without including the mean or the trend. The solar annual and semiannual tides were omitted from the tidal harmonic predictions because harmonic analyses do not always represent the seasonal sea level cycle well, and most of the seasonal signal is actually driven by nontidal effects that have an influence on MSLA. Treatment of the seasonal sea level cycle is discussed below.
3) The tide was subtracted from the raw sea level record to obtain a nontidal residual sea level.
4) MSLA was obtained by removing the linear trend, subtracting the mean over the entire record, and low-pass filtering the nontidal residual sea level using a 32-day (1 month) cutoff threshold, following the orthogonal wavelet decomposition method of Goring (2008). The resulting MSLA time series were relative to a mean sea level of zero with no long-term trend and contained only sea level variability greater than or equal to one month. MSLA is also commonly calculated from the mean of the nontidal residual sea level, averaged over a 1-month period (e.g., Chowdhury et al. 2007). This method includes shorter-period sea level variability induced by synoptic weather systems. Both techniques were tested and give similar results, and development of the high-water alert calendar is insensitive to this choice.

The tide and MSLA time series were further decimated to times of peak high tide, since coastal inundation hazard is greatest at high tide. MSLA varies slowly compared with the tide and decimating MSLA to peak high-tide makes negligible difference to the observed MSLA distribution, but it is convenient for data handling, as it reduces both high tide and MSLA time series to the same dimension.

The tide and MSLA data are presented with the mean removed, relative to a mean sea level of zero (MSL = 0). In this way the analysis methods are demonstrated without reference to gauge zero or local datum. To convert from MSL = 0 to local datum, an MSL datum offset must be subsequently applied as described above.

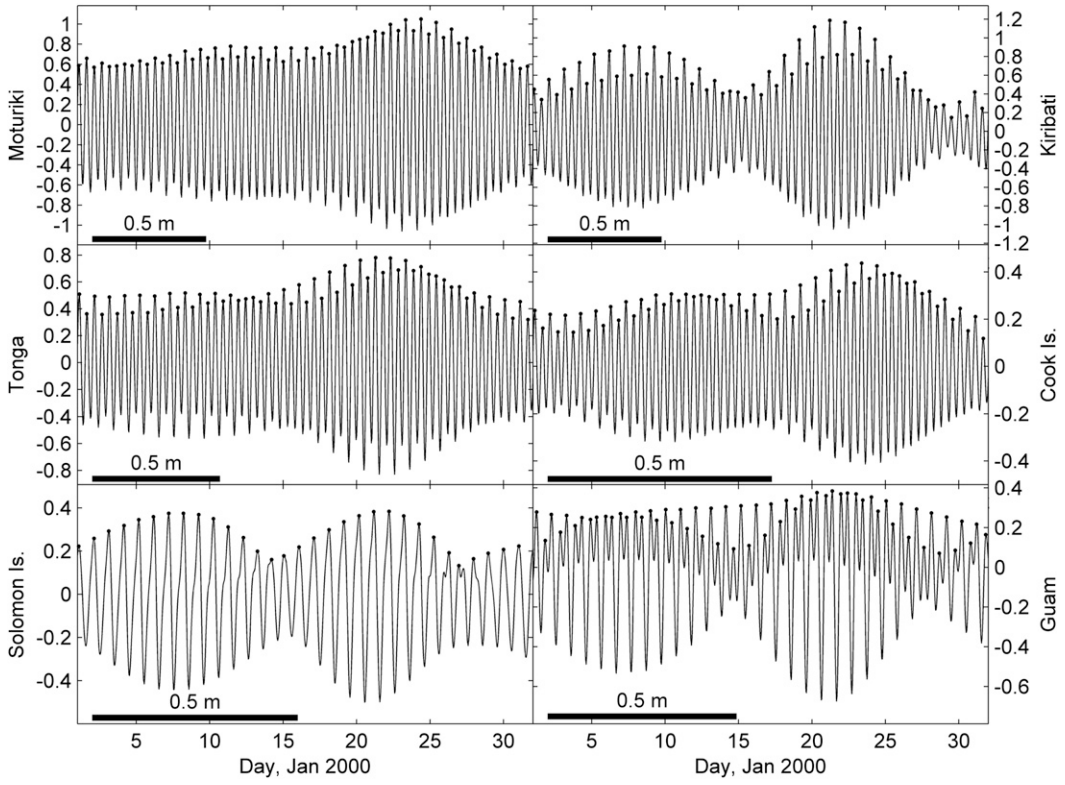

FIG. 3. Harmonic tide predictions for January 2000 at six locations. The scale bar marks 0.5-m tide range. Dots mark high waters.

d. Handling of seasonal cycle

Statistical forecasts of MSLA require that data are stationary, but most climate data exhibit cyclostationary features because of the seasonal nature of climate (Chowdhury et al. 2007). Thus, Chowdhury et al. 2007 removed the mean seasonal sea level cycle to leave only the stochastic residual when modeling MSLA, before reintroducing it to their seasonal sea level outlooks. The dynamic model of Miles et al. (2014) includes seasonal dynamic effects on MSLA. The seasonal sea level cycle includes the gravitational solstice tides Sa and Ssa, which are aliased with seasonal steric and atmospheric effects. The seasonal semiannual Ssa tide is produced by the declination of the sun's apparent orbit relative to the earth's equatorial plane, and the seasonal annual Sa tide is produced by the elliptical orbit of the earth around the sun. However, solstice tides for most practical purposes would be too small to worry about except that they are not just produced by solar gravity; they get a boost from other effects that follow the sun's seasonal cycles, such as solar heating of the oceans and changes in the circulation in the atmosphere (Boon 2013). The nontidal seasonal sea level response to atmospheric and steric effects is less regular and predictable than the gravitational effects of the moon and sun, which control other tidal constituents. Annual tidal harmonic analyses show that the amplitude and phase of Sa and Ssa harmonics change considerably at all sites from year to year; for example, the median Sa and Ssa amplitude ranges were 0.06 and 0.10 m, respectively (where the ranges were calculated over all years in each record, and the median was subsequently calculated from the ranges at all 17 locations). While they can be determined retrospectively *for a given year or years*, they cannot be precisely forecast from previously determined harmonics. Furthermore, the seasonal sea level cycle is not accurately resolved by sinusoidal Sa and Ssa harmonics, although they provide a reasonable representation at some locations (e.g., Chowdhury et al. 2007). An alternative nonharmonic method is to calculate the mean monthly MSLA. Whereas the mean seasonal cycle needs to be separated, then reintroduced during statistical MSLA forecasts (Chowdhury et al. 2007), it can be left in the MSLA time series for the purposes of calculating high-water alert thresholds. The treatment of the mean seasonal cycle is not crucial to the calculation of high-water alert thresholds, since they are created from the summed sea level components. For example, at sites where the Sa and Ssa harmonics provide a good

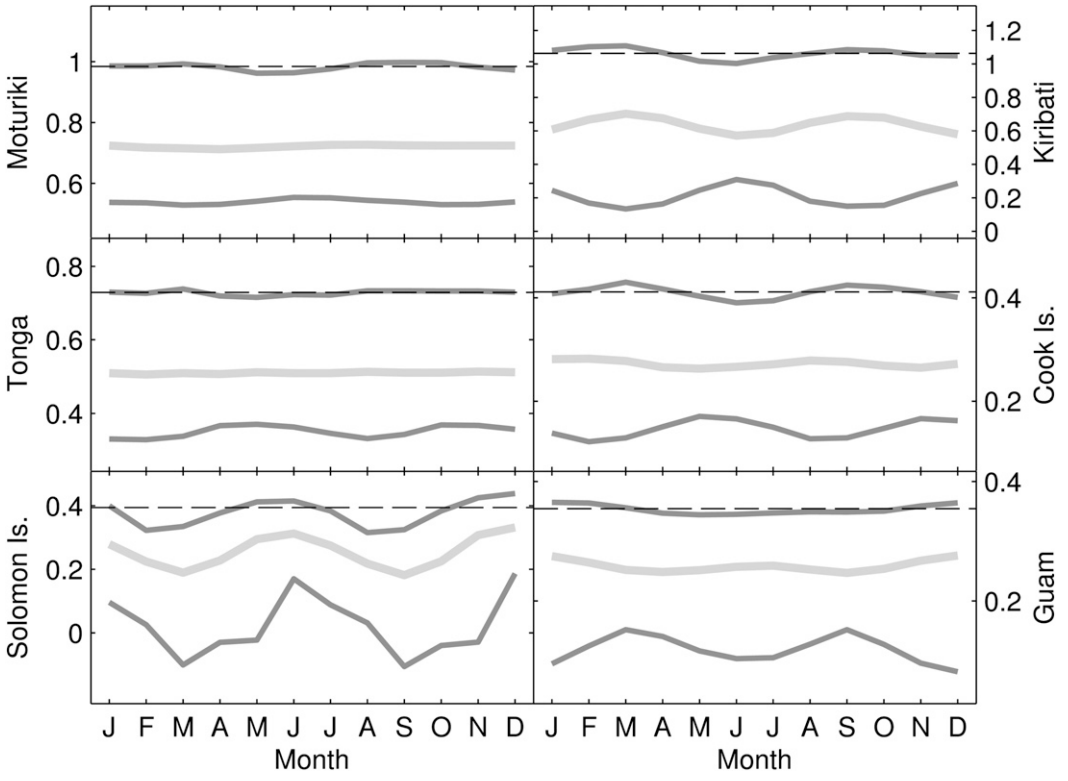

FIG. 4. Monthly average high-tide statistics (m) for six locations. The thick light line indicates the median, intermediate gray line indicates the 5th and 95th percentiles, and the black dashed line shows epoch-averaged 95th percentile. Note that the epoch varies for each sea level record.

representation of the mean seasonal cycle, the seasonal cycle could have been included in the tide predictions rather than the MSLA. However, because the mean seasonal cycle is included in MSLA forecasts (Chowdhury et al. 2007; Miles et al. 2014), the tidal predictions used to implement the high-water calendar should not include the solstice tides, because seasonal MSLA estimates are included in the seasonal MSLA outlooks.

3. Results

Table 2 shows statistics of tide and MSLA at all 17 locations. The tide regime varies throughout the PIR and New Zealand—from a tidal range of 0.81 at Rarotonga, of the Cook Islands, to 3.13 at Auckland—and includes semidiurnal (twice daily), mixed, and diurnal (once daily) regimes. Note that the tidal and MSLA range was defined in terms of the difference between the 0.5 and 99.5 percentiles of each record. The K_1 diurnal tide (among others) is influential at all sites (although not always one of the largest three constituents; Table 2), leading to mixed semidiurnal regimes rather than pure semidiurnal regimes, whereby the high-tide amplitudes "beat," with one high tide per day being higher than the other. Within the semidiurnal regimes, there are regimes where the S_2 constituent is approximately double N_2, leading to a classical semidiurnal spring–neap regime with two springs and neaps of approximately equal amplitude per month [Kiribati (Fig. 3), Marshall Islands, Tuvalu]. At these sites the nautical ($M_2 + S_2$) definition of MHWS would be appropriate. There are semidiurnal sites where the N_2 constituent is approximately equivalent to S_2, leading to the perigean regime with a single dominant spring tide per month [Auckland, Moturiki (Fig. 3), Tonga (Fig. 3), Cook Islands (Fig. 3), Fiji, Samoa]. At these sites the MHWPS ($M_2 + S_2 + N_2$) definition of MHWS would apply. There are mixed tidal regimes where the diurnal constituents are similar in magnitude to the semidiurnal tides, with the relative importance of the diurnal and semidiurnal components changing throughout the month [Yap, Guam (Fig. 3), and Vanuatu]. There are two diurnal regimes in Papua New Guinea and the Solomon Islands (Fig. 3). The changing tide regimes show that it would be difficult to consistently define MHWS or a red-alert threshold based on a tidal harmonic definition, necessitating the use of the tide exceedance curve.

The MSLA range is up to ~0.5 m in some locations, which can be a significant proportion of the total high-water

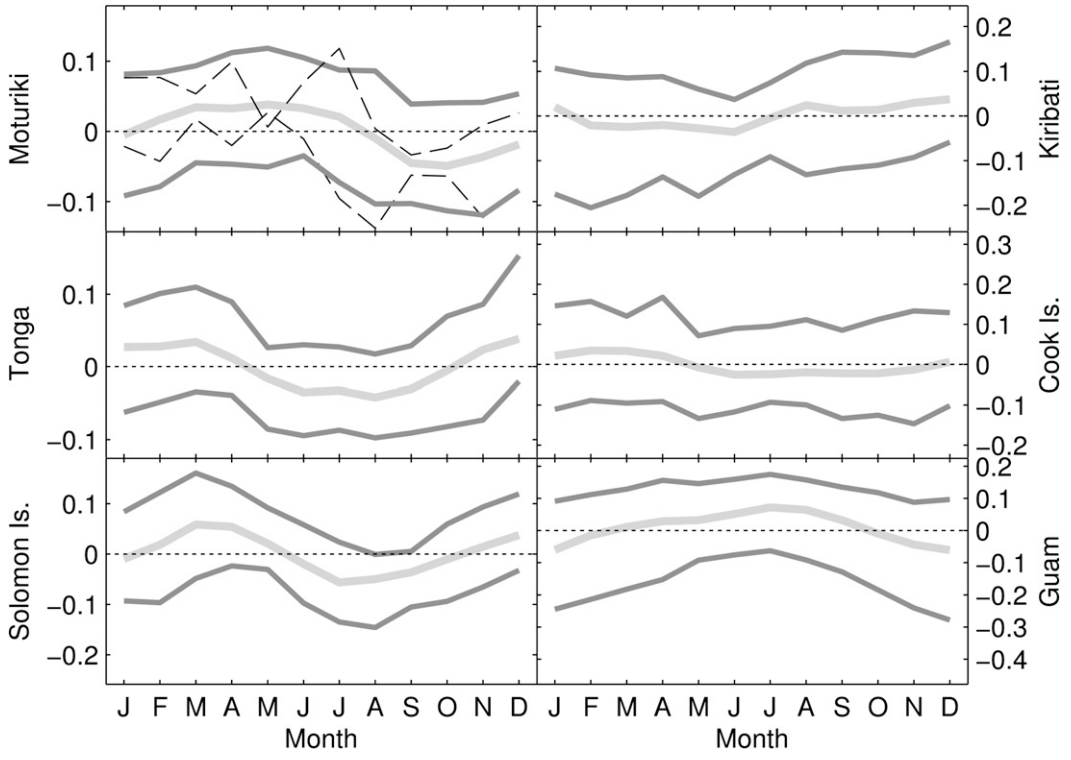

FIG. 5. Monthly average MSLA statistics (m) for six locations. The thick light line indicates the mean annual cycle and the intermediate gray lines indicate the 5th and 95th percentiles. For Moturiki only, the mean annual cycles for 1994 (bottom dashed line) and 1999 (top dashed line) have been superimposed.

elevation; for example, the ratio of the 95th percentile elevations of MSLA relative to the 95th percentile high tide was 41% at Guam (Table 2). The MSLA range tends to be largest in the western Pacific.

Data are plotted from six sites (Moturiki, Kiribati, Tonga, Cook Islands, Solomon Island, and Guam) that contain a range of tidal regime, tidal range, and MSLA range (Fig. 3). They give a fair representation of the behavior of both tide and MSLA components throughout the region, and of their interaction. For example, Kiribati is similar to the Marshall Islands, Yap and Vanuatu are similar to Guam, Papua New Guinea is similar to the Solomon Islands, and Auckland is similar to Moturiki.

Figure 4 shows monthly averaged high-tide statistics at six locations. Aside from the tidal range varying between locations, Fig. 4 shows that there is seasonality in the high-tide range and variance. In many of the studied locations, the highest high tides (demonstrated using the 95th percentile) are more likely to occur at certain times of the year, as a result of the relative phasing of diurnal (e.g., K_1) and semidiurnal S_2 tidal harmonics. Therefore, the epoch-averaged 95th percentile high-tide elevation at times underpredicts or overpredicts the monthly average 95th percentile probability of exceedance.

Figure 5 shows the monthly averaged MSLA statistics at six locations. MSLA also displays seasonality in both the mean cycle and in variance. There is considerable interannual variability around the mean seasonal cycle, as demonstrated for the years 1994 (low MSLA) and 1999 (high MSLA) at Moturiki. Despite the pronounced mean seasonal cycle, instantaneous MSLA can be positive or negative in any month of the year. Thus, whereas the tide is deterministic, MSLA is cyclostationary in that it is a stochastic process (not deterministic) but has statistical properties that vary periodically with time.

Figures 4 and 5 show that although high tide and MSLA are not physically coupled, they have seasonal cycles that can covary and are thus not statistically independent. This has implications for the development of alert thresholds for the joint distribution of high tide plus MSLA—for which the dependence should theoretically be accounted. This was achieved here by using the empirical time series of the summed components. However, there may be situations where it would be useful to treat high tide and MSLA as independent variables. One such situation might be where only a short gauge record is available to obtain an empirical MSLA record (e.g., one year), but tidal harmonic constituents enable much longer tidal time series to be predicted and thus a more

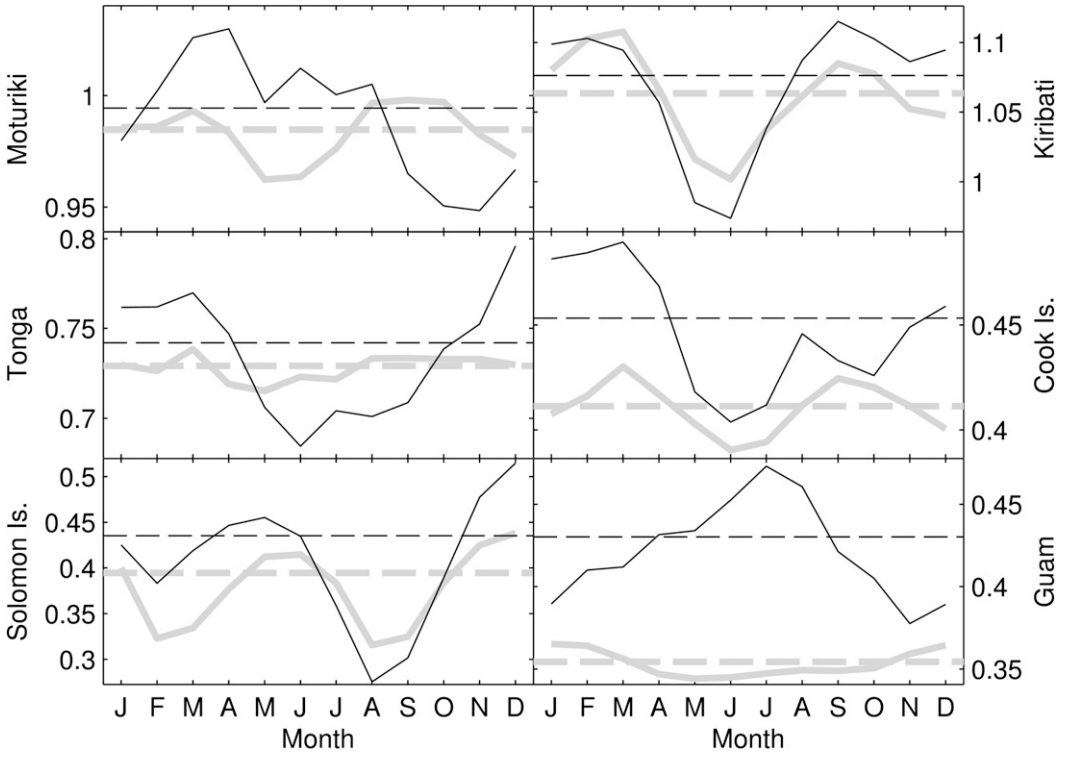

FIG. 6. Monthly average 95th percentile of high tide and high tide plus MSLA (m) for six locations. The light gray solid line shows the monthly average 95th percentile of high tide, the black solid line shows the monthly average 95th percentile of high tide plus MSLA, the light gray dashed line indicates the epoch-average 95th percentile of high tide, and the black dashed line shows the epoch-average 95th percentile of high tide plus MSLA.

accurate definition of the high-tide exceedance curve. We convolved the independent distributions of high tide and MSLA to obtain a joint probability distribution for high water under the false pretense that the two distributions were independent. The resulting epoch-averaged 90%, 95%, and 99% exceedance elevations were less than 1% different from those obtained from the empirical joint exceedance distribution at the great majority of locations and were less than 2% different (<1 cm) at all locations. Thus, for the purposes of obtaining practical high-water exceedance elevations at the studied locations, the covariance of high tide and MSLA can be ignored and the two independent distributions convolved to obtain a joint probability cumulative exceedance distribution.

Figure 6 shows the monthly average 95th percentile of high tide and high water (that includes MSLA), along with epoch-averaged 95th percentile elevations. Figure 6 shows that the addition of MSLA to high tide influences both the mean seasonal distribution of sea level elevation and the value of epoch-averaged sea level elevation thresholds by changing the joint cumulative exceedance distribution (as in Fig. 1, for example). The plots suggest that by not including MSLA, the associated alert thresholds for high water could also be impractical (too low) if based on high tide alone. The epoch-averaged high-water threshold reflects the influence of both processes. Furthermore, a high-tide alert calendar could give a false impression of the true high-water elevation. An epoch-averaged high-water threshold will be more regularly exceeded on average, in given seasons, because of mainly climatic effects on MSLA, compounded by tidal seasonality.

Figure 7 explores the relationships between tide, MSLA, and the change in the number of exceedances of a high-tide threshold due to inclusion of MSLA. The ratio of the 95th percentile exceedance elevations of MSLA relative to those of high tide increases from left to right (Fig. 7, top plot). The plot second from the top shows the percent increase in the number of high-water peaks that exceed the elevation of the 95th percentile of high tide alone, once MSLA is added. As MSLA becomes increasingly large compared to tide, its inclusion causes more and more high-water elevations to exceed the 95th percentile high-tide (only) alert threshold. In other words, the addition of MSLA causes many more high-water threshold exceedances than predicted from tides alone. MSLA has more influence on high water, and thus on the choice of a practical high-water alert threshold, at sites plotted toward the

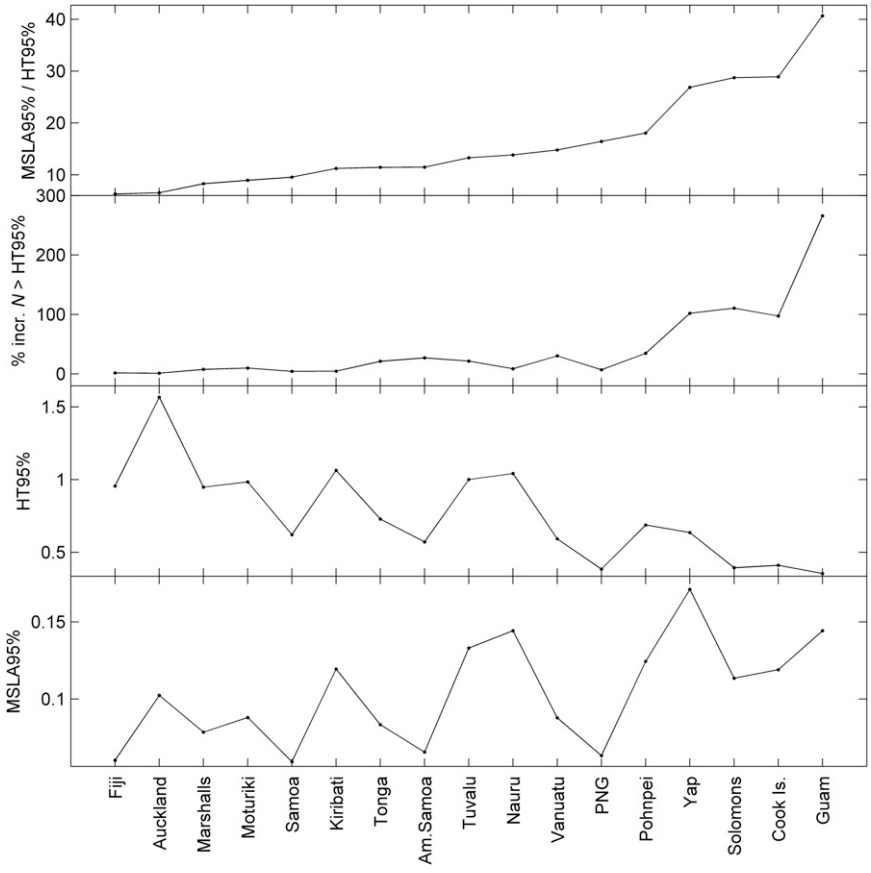

FIG. 7. High tide and MSLA statistics for 17 locations. (from top to bottom) Ratio of epoch-average 95th percentile of MSLA (MSLA95%) and 95th percentile high tide (HT95%); percent increase in the number of high-water peaks (N) that exceed the elevation of the 95th percentile of high tide alone once MSLA is added; epoch-average 95th percentile of high-tide; and epoch-average 95th percentile of MSLA.

right of Fig. 7. Sites plotted to the right generally have lower tidal and higher MSLA range.

Figure 8 (Guam) and Fig. 9 (Kiribati) show examples of one form of high-water alert calendar, where high-water alert thresholds have been superimposed onto actual total sea level time series, and the high-water peaks exceeding those thresholds have been identified. In both figures, the top plot shows a month where background MSLA was high (+0.15 m at Guam, +0.18 m in Kiribati), while the bottom plot shows a month where MSLA was approximately zero. The tides have similar amplitudes in both months, but the number of high-water alerts is much greater during the months with high MSLA, which shows the importance of MSLA in raising high-water elevations above alert levels at both sites.

Figure 10 presents another form of high-water alert calendar, the purpose of which is to compare and contrast the effect of various MSLA elevations on high-water alerts. In Fig. 10, the high-water alert thresholds for the actual measured high-water peaks at a time of higher MSLA are presented on the left, with scenarios for zero MSLA plotted in the middle and a negative MSLA on the right. Figures 8–10 demonstrate the following:

- The high-tide alert calendar instantly conveys the dates that high-tide peaks are expected to be higher than given thresholds, and the color shading clearly conveys the severity of the alert.
- Inclusion of MSLA in the high-tide calendar can be important even for sites like Tarawa in Kiribati, where tides dominate sea level variability (Fig. 7). In this March 1997 example, the number of high-water alert days in Kiribati more than doubled, from 6 to 13, compared to a zero-MSLA scenario. Had MSLA been negative, then the high-water alerts almost disappear.
- Locations with a relatively small tidal range and large MSLA fluctuations can be highly sensitive to MSLA fluctuations, such as at Guam. Large climate-driven MSLA displacements can result in persistently high-tide

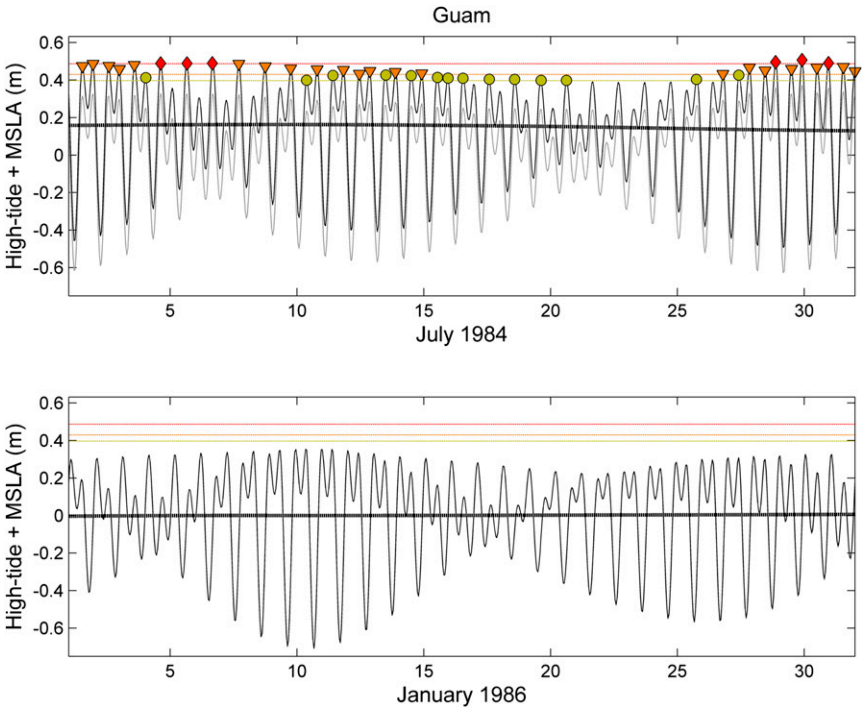

FIG. 8. Predicted tide-plus-measured MSLA at Guam. The light gray line shows the predicted tide, the thin black line shows the tide plus MSLA, and the bold line indicates MSLA. Alert levels and high-water peak alerts are marked in yellow, orange, and red for the the 90th, 95th, and 99th percentiles, respectively.

peaks for most of the month. In this July 1984 example, the +0.15-m MSLA resulted in high-tide peaks in excess of the 90% (yellow) alert level for most of the month, the 95% (orange) alert level or above for 20 days of the month, and the 99% (red) alert level for 6 days. With a background MSLA of zero or less, there would have been no high-water alerts.

4. Discussion and conclusions

Tides are routinely predictable throughout the Pacific via tidal harmonic analysis of sea level gauge records or global ocean tide models (e.g., Egbert and Erofeeva 2002; Lyard et al. 2006; Matsumoto et al. 2000; Ray 1999). Thus, the red-alert tide calendar concept, developed for New Zealand's semidiurnal tidal regime (Bell 2010), can be applied throughout the Pacific as a mechanism for presenting an early warning a few months ahead of an increased risk of potential high-tide-related inundation. The New Zealand red-alert calendar targets the dates of perigean spring tides, when the sun and moon's gravitational forces align at the same time that the moon is closest to the earth in its orbit. The present work defines alert thresholds (which can be defined to suit the particular location) based on empirical high-water exceedance curves rather than thresholds based on a combination of specific tidal harmonic constituents. The high-tide exceedance curves can be applied universally to all locations to define alert thresholds and have the advantage of being independent from the dominant astronomical components at a specific location, which vary according to the local tidal regime.

While a high-tide alert calendar can be derived from knowledge of tides alone, the inclusion of MSLA enhances the prediction of high-water alert levels, with a more realistic connection to what actually occurs or is observed. This is most significant at locations such as Guam, where MSLA variability is similar in magnitude to high-tide variability; however, all of the locations studied would benefit from inclusion of MSLA forecasts in the high-water alerts. At times of high or low MSLA, a high-tide alert calendar would be unrealistic if it did not account for MSLA. Likewise, the alert thresholds for high water would be impractical if based on high tide alone.

High-water exceedance curves provide a framework for combining high tide and MSLA to identify the joint probability of exceedance of combined high-water elevations. They could also be used to assess the increase in frequency of high waters exceeding present-day thresholds from a specified sea level rise, with the assumption

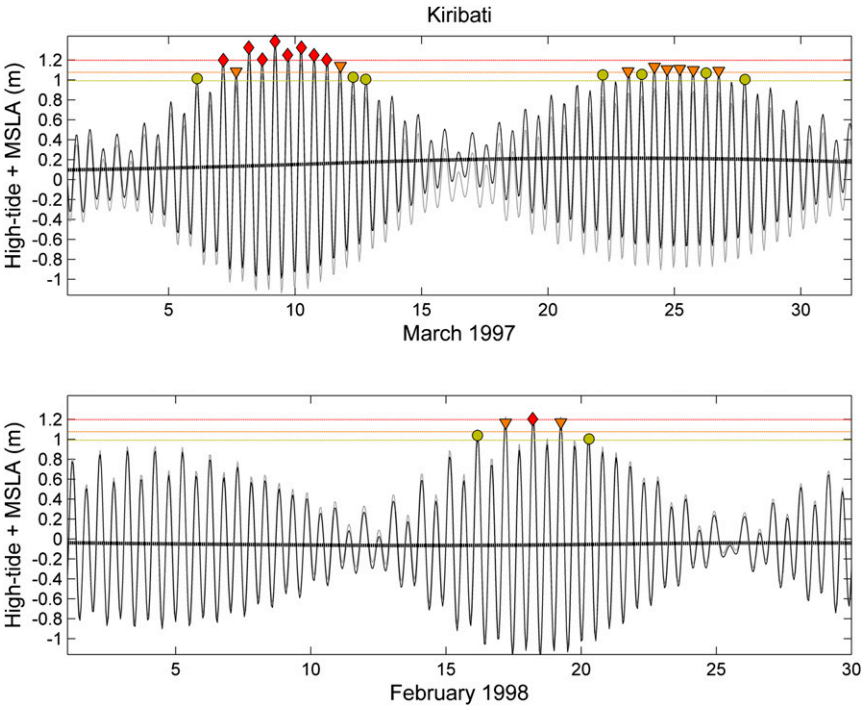

FIG. 9. Predicted tide-plus-measured MSLA at Kiribati. The light gray line shows the predicted tide, the thin black line shows the tide plus MSLA, and the bold line indicates MSLA. Alert levels and high-tide peak alerts are marked in yellow, orange, and red for the 90th, 95th, and 99th percentiles, respectively.

that future modification to tidal characteristics is relatively small. In this case the entire high-tide exceedance curve can be raised vertically by the equivalent amount of sea level rise added to the present-day MSL (Bell 2010).

The high-water alert calendar concept has been demonstrated here using sea level gauge records with a minimum length of 19.7 years (Table 1). Records of this length include several ENSO cycles and multiple seasonal cycles and so provide a fair representation of MSLA, alongside comprehensive tidal harmonic analysis. The authors recently developed a high-water alert calendar for the island of Kosrae, where the only sea level record was just over 1-yr long at the time of implementation. This is sufficient to give reasonable tidal predictions based on harmonic analysis, but is not long enough to robustly define the distribution of MSLA. A pragmatic solution was to obtain MSLA records from analysis of surrounding sea level gauges at Nauru, Pohnpei, and the Majuro, and assume that the average of these would provide a reasonable representation of MSLA at Kosrae. The mean MSLA distribution was convolved with the distribution of tidal predictions (under the assumption of independence) to calculate high-water alert thresholds. The high-water alert thresholds were combined with tidal predictions and Pacific ENSO Applications Climate Center seasonal sea level (MSLA) outlook from the nearest location, to implement a pragmatic (if not precise) high-water alert calendar (http://kosraecoast.com). Despite the limiting assumptions, the inclusion of MSLA predictions makes the high-water calendar more realistic and enhances its value to end users. This example shows that the high-water calendar can be implemented to accommodate practical constraints—the key point being that inclusion of MSLA adds practical value to high-tide predictions.

For many Pacific Islands, coastal inundation (not including intense tropical cyclone or tsunami events) most commonly occurs due to a combination of high tide levels occurring at the same time as moderate swell conditions. These effects are compounded by climate-related effects on MSLA. The MSLA-adjusted high-water calendar is a practical tool to predict dates of higher-than-normal high tides, when low-lying land is particularly vulnerable to inundation. The calendar is highly visual and easily interpreted without requiring significant technical expertise or ingestion or interpretation of large amounts of data or text. The provision of several alert thresholds is designed to allow end users to use their experience to ''tune in'' to the calendar, by correlating the alert level with the severity of consequences. Thus, the high-water calendar can be used, for example, by local fishermen making decisions on where to moor vessels, or by a trained

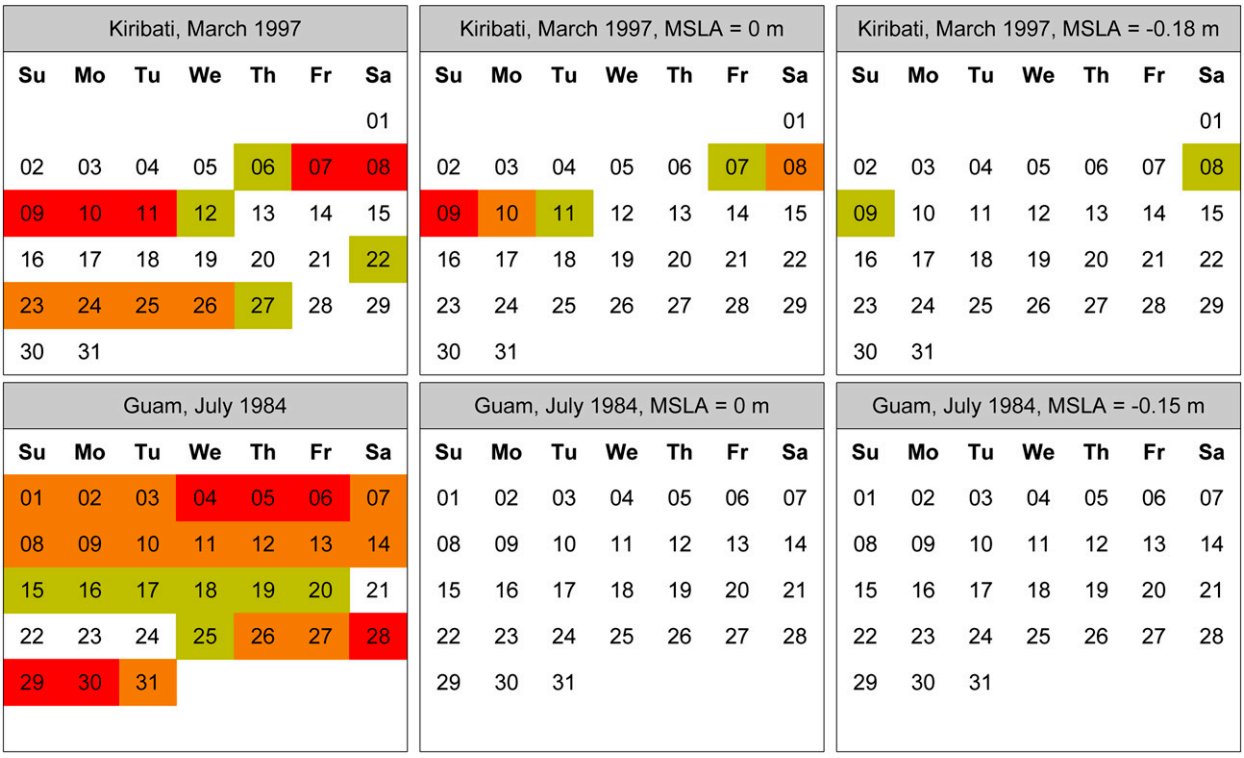

FIG. 10. Shaded high-water alert calendar for (top) March 1997 at Guam and (bottom) July 1984 at Tarawa in Kiribati. Calendars show (left) the actual measured sea levels, as per Figs. 8 and 9; (middle) the high-water alerts if MSLA had been zero; and (right) the high-water alerts if the measured MSLA had been negative instead of positive.

emergency manger, knowing that even a moderate swell event could cause significant inundation if arriving on a red-alert date. The high-water calendar is easily updated when new MSLA forecasts become available (typically 1–3 months ahead) and can be displayed on a website or faxed for local distribution.

Acknowledgments. The project was funded by the New Zealand Ministry of Business, Innovation, and Employment under Core Project CLCP1305 and Research Project HAFS1403 of the National Institute of Water and Atmospheric Research. Thanks to Drs. Graham McBride, Emily Lane, and Melisa Menendez for the stimulating discussions on the subject of joint probability. Thanks to Benjamin Robinson for processing of sea level data. Sea level data were obtained from the University of Hawaii Sea Level Center funded by the National Ocean Service of the National Oceanic and Atmospheric Administration, with support from the Joint Archive for Sea Level, which is a cooperative effort between the U.S. National Oceanographic Data Center and the University of Hawaii Sea Level Center. Sea level data were obtained from the Australian Bureau of Meteorology Pacific Sea Level Monitoring Project website. Sea level data for Auckland were supplied by Port of Auckland Ltd. We are grateful for the insightful comments of two anonymous reviewers that helped us to improve the manuscript.

REFERENCES

Becker, M., B. Meyssignac, C. Letetrel, W. Llovel, A. Cazenave, and T. Delcroix, 2012: Sea level variations at tropical Pacific islands since 1950. *Global Planet. Change,* **80–81,** 85–98, doi:10.1016/j.gloplacha.2011.09.004.

Bell, R. G., 2010: Tidal exceedances, storm tides and the effect of sea-level rise. *Proc. 17th Congress of the Asia and Pacific Division of the Int. Association of Hydraulic Engineering and Research,* Auckland, New Zealand, IAHR, 2b001.

Boak, E. H., and I. L. Turner, 2005: Shoreline definition and detection: A review. *J. Coastal Res.,* **21,** 688–703, doi:10.2112/03-0071.1.

Boon, J. D., 2013: *Secrets of the Tide: Tide and Tidal Current Analysis and Predictions, Storm Surges and Sea Level Trends*. Elsevier, 224 pp.

Chowdhury, MD. R., P.-S. Chu, T. Schroeder, and N. Colasacco, 2007: Seasonal sea-level forecasts by canonical correlation analysis—An operational scheme for the U.S.-affiliated Pacific Islands. *Int. J. Climatol.,* **27,** 1389–1402, doi:10.1002/joc.1474.

Chu, P. S., and J. X. Wang, 1998: Modeling return periods of tropical cyclone intensities in the vicinity of Hawaii. *J. Appl. Meteor.,* **37,** 951–960, doi:10.1175/1520-0450(1998)037<0951:MRPOTC>2.0.CO;2.

Diamond, H. J., A. M. Lorrey, K. R. Knapp, and D. H. Levinson, 2012: Development of an enhanced tropical cyclone tracks database for the southwest Pacific from 1840 to 2010. *Int. J. Climatol.,* **32,** 2240–2250, doi:10.1002/joc.2412.

Egbert, G. D., and S. Y. Erofeeva, 2002: Efficient inverse modeling of barotropic ocean tides. *J. Atmos. Oceanic Technol.,* **19,** 183–204, doi:10.1175/1520-0426(2002)019<0183:EIMOBO>2.0.CO;2.

Foreman, M. G. G., J. Y. Cherniawsky, and V. A. Ballantyne, 2009: Versatile harmonic tidal analysis: Improvements and applications. *J. Atmos. Oceanic Technol.,* **26,** 806–817, doi:10.1175/2008JTECHO615.1.

Goring, D. G., 2008: Extracting long waves from tide-gauge records. *J. Waterw. Port Coastal Ocean Eng.,* **134,** 306–312, doi:10.1061/(ASCE)0733-950X(2008)134:5(306).

——, S. A. Stephens, R. G. Bell, and C. P. Pearson, 2011: Estimation of extreme sea levels in a tide-dominated environment using short data records. *J. Waterw. Port Coastal Ocean Eng.,* **137,** 150–159, doi:10.1061/(ASCE)WW.1943-5460.0000071.

Hoeke, R. K., K. L. McInnes, J. C. Kruger, R. J. McNaught, J. R. Hunter, and S. G. Smithers, 2013: Widespread inundation of Pacific islands triggered by distant-source wind-waves. *Global Planet. Change,* **108,** 128–138, doi:10.1016/j.gloplacha.2013.06.006.

Jay, D. A., 2009: Evolution of tidal amplitudes in the eastern Pacific Ocean. *Geophys. Res. Lett.,* **36,** L04603, doi:10.1029/2008GL036185.

Lyard, F., F. Lefevre, T. Letellier, and O. Francis, 2006: Modelling the global ocean tides: Modern insights from FES2004. *Ocean Dyn.,* **56,** 394–415, doi:10.1007/s10236-006-0086-x.

Matsumoto, K., T. Takanezawa, and M. Ooe, 2000: Ocean tide models developed by assimilating TOPEX/POSEIDON altimeter data into hydrodynamical model: A global model and a regional model around Japan. *J. Oceanogr.,* **56,** 567–581, doi:10.1023/A:1011157212596.

Merrifield, M. A., P. R. Thompson, and M. Lander, 2012: Multidecadal sea level anomalies and trends in the western tropical Pacific. *Geophys. Res. Lett.,* **39,** L13602, doi:10.1029/2012GL052032.

——, A. S. Genz, C. P. Kontoes, and J. J. Marra, 2013: Annual maximum water levels from tide gauges: Contributing factors and geographic patterns. *J. Geophys. Res. Oceans,* **118,** 2535–2546, doi:10.1002/jgrc.20173.

Miles, E. R., C. M. Spillman, J. A. Church, and P. C. McIntosh, 2014: Seasonal prediction of global sea level anomalies using an ocean–atmosphere dynamical model. *Climate Dyn.,* **43,** 2131–2145, doi:10.1007/s00382-013-2039-7.

Müller, M., 2011: Rapid change in semi-diurnal tides in the North Atlantic since 1980. *Geophys. Res. Lett.,* **38,** L11602, doi:10.1029/2011GL047312.

Nicholls, R. J., and A. Cazenave, 2010: Sea-level rise and its impact on coastal zones. *Science,* **328,** 1517–1520, doi:10.1126/science.1185782.

Nurse, L., and Coauthors, 2014: Small islands. *Climate Change 2014: Impacts, Adaptation, and Vulnerability; Part B: Regional Aspects,* V. R. Barros et al., Eds., Cambridge University Press, 1613–1654.

Pugh, D. T., 1987: *Tides, Surges and Mean Sea-Level: A Handbook for Engineers and Scientists.* John Wiley & Sons Ltd., 486 pp.

——, 2004: *Changing Sea Levels: Effects of Tides, Weather and Climate.* Cambridge University Press, 280 pp.

Rasheed, A. S., and V. P. Chua, 2014: Secular trends in tidal parameters along the coast of Japan. *Atmos.–Ocean,* **52,** 155–168, doi:10.1080/07055900.2014.886031.

Ray, R. D., 1999: A global ocean tide model from TOPEX/Poseidon altimetery: GOT99.2. NASA Tech. Memo. NASA/TM—1999-209478, 58 pp.

Sasaki, Y. N., S. Minobe, N. Schneider, T. Kagimoto, M. Nonaka, and H. Sasaki, 2008: Decadal sea level variability in the South Pacific in a global eddy-resolving ocean model hindcast. *J. Phys. Oceanogr.,* **38,** 1731–1747, doi:10.1175/2007JPO3915.1.

Sinclair, M. R., 2002: Extratropical transition of southwest Pacific tropical cyclones. Part I: Climatology and mean structure changes. *Mon. Wea. Rev.,* **130,** 590–609, doi:10.1175/1520-0493(2002)130<0590:ETOSPT>2.0.CO;2.

Stammer, D., A. Cazenave, R. M. Ponte, and M. E. Tamisiea, 2013: Causes for contemporary regional sea level changes. *Annu. Rev. Mar. Sci.,* **5,** 21–46, doi:10.1146/annurev-marine-121211-172406.

Terry, J. P., and G. Gienko, 2010: Climatological aspects of South Pacific tropical cyclones, based on analysis of the RSMC-Nadi (Fiji) regional archive. *Climate Res.,* **42,** 223–233, doi:10.3354/cr00912.

Timmermann, A., S. McGregor, and F.-F. Jin, 2010: Wind effects on past and future regional sea level trends in the southern Indo-Pacific. *J. Climate,* **23,** 4429–4437, doi:10.1175/2010JCLI3519.1.

Walters, R. A., D. G. Goring, and R. G. Bell, 2001: Ocean tides around New Zealand. *N. Z. J. Mar. Freshwater Res.,* **35,** 567–579, doi:10.1080/00288330.2001.9517023.

Woodworth, P. L., 2010: A survey of recent changes in the main components of the ocean tide. *Cont. Shelf Res.,* **30,** 1680–1691, doi:10.1016/j.csr.2010.07.002.